CALICE Analysis Note CAN-011c; Addendum C
April 28, 2009

Preliminary Results on Lateral Profiles in Hadron Showers Reconstructed with the CALICE Tile AHCAL Prototype

R. Fabbri, A. Lucaci-Timoce
for the CALICE Collaboration

1 Introduction

Due to the high granularity, of the Analogue Hadronic Calorimeter (AHCAL) prototype, designed and developed by the CALICE Collaboration, the development of hadronic showers can be studied in great detail. Results on longitudinal shower profiles in data, and comparisons with the available GEANT4 models were already discussed in [1].

This note presents the preliminary analysis of lateral energy profiles in hadron showers reconstructed in the AHCAL prototype. In addition, the fractional energy deposited in the whole calorimeter, as a function of the shower radius, is investigated. The mean shower radius is studied as well. Monte Carlo simulations, performed using different models, and including detector and physics effects, are compared with the data.

2 Data and Monte Carlo Samples

In this work, data accumulated during the test-beam operations at CERN in 2007, with beam normal to the AHCAL, are analysed. All the three CALICE calorimeter prototypes (ECAL, AHCAL and TCMT) were present on the beamline. Only the analysis of the 18 GeV π^- test-beam data is presented here. The investigation of other test-beam energy data is ongoing. The data were reconstructed using the up-to-date calibration.

For the Monte Carlo comparison, two different models which are the most discrepant in terms of energy deposition [1] are considered: LHEP and QGSP_BERT [2]. Note that in the QGSP_BERT model, the interactions of low energy particles are described by the Bertini cascade (0 GeV $< E < 9.9$ GeV) and by the low energy parameterisation LEP (9.5 GeV $< E < 25$ GeV), whereas the actual quark string model implemented in QGSP starts to act only at higher energies ($E > 12$ GeV). Monte Carlo events were generated using the latest Mokka version (mokka-06-07-p03-calice) [3], based on the latest GEANT4 version (9.2) [4], which includes Birks law [5]. For each model, 100000 events were generated.

The latest Monte Carlo digitisation software was used, including a time cut (150 ns) due to the AHCAL pulse-shaping electronics windows [6], which is expected to reduce

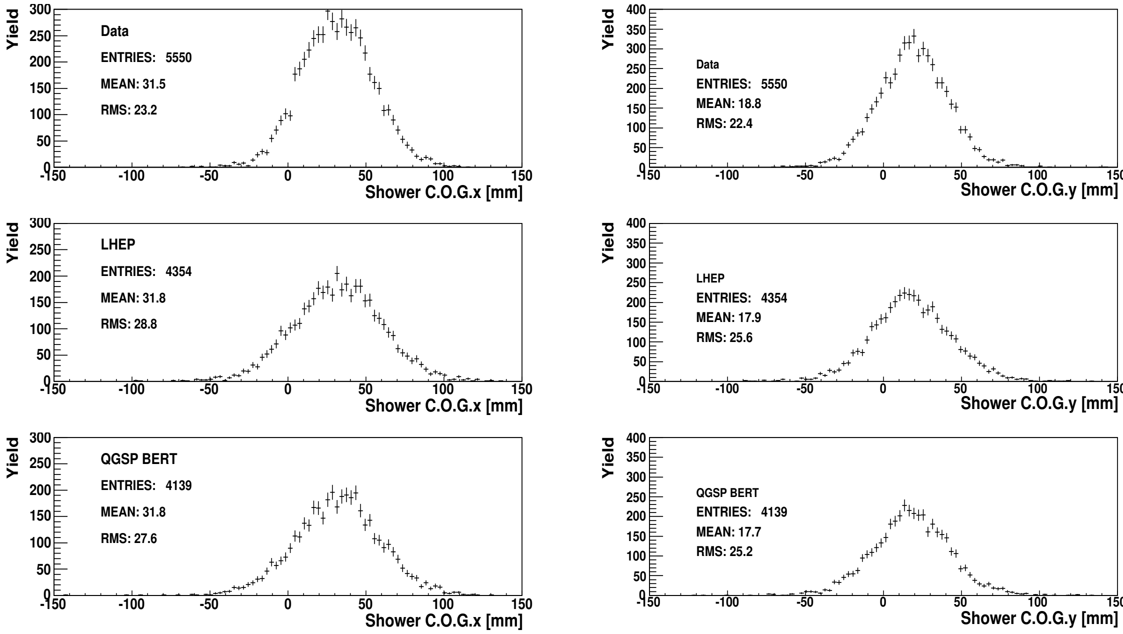

Figure 1: *The beam profile distributions in the front face of the AHCAL, represented via the shower energy center of gravity distributions, are presented for both data and Monte Carlo.*

the number of neutrons depositing energy in the AHCAL, since they usually come later than the majority of the particles.

The properties of the beam used in the simulation were determined from the real test-beam data. The beam position was set to position of the shower energy center of gravity measured in the AHCAL. The beam spread was taken from the beam profile width reconstructed in the drift chamber most upstream, and the beam gun was placed in front of this chamber. The beam profile distributions in the front face of the AHCAL, represented via the shower energy center of gravity distributions, are presented in Fig. 1 for both data and Monte Carlo. The beam position reproduced by the simulation is almost the same as in real data, whereas beam spread differences up to 5 mm are observed. However, Monte Carlo studies indicate that beam width values larger than 15 mm have negligible effects in correctly reconstructing lateral profiles [7].

3 Event Selection

Only the beam type events are selected, whereas calibration and pedestal events are rejected. Showers developing in the AHCAL-TCMT system only are considered in this work. Showers starting already in the ECAL are removed from the analysis considering only events with less than 50 hits in the ECAL, see Fig. 2.

To reduce noise in the AHCAL, only calorimeter tiles with a reconstructed signal above 0.5 MIPs are considered.

Visible MIPs in the AHCAL are removed by discarding events with less than 150 hits. This cut is based on the distribution of the number of hits in the AHCAL versus the number of hits in the TCMT, see Fig. 3. The effect of this selection is visible in the hit distribution in the TCMT, shown in Fig. 4. Before applying the above cut, the muon peak is visible at around 25 hits, while this is removed after applying the mentioned event selection. On top of this cut, an additional selection is applied to discard possible

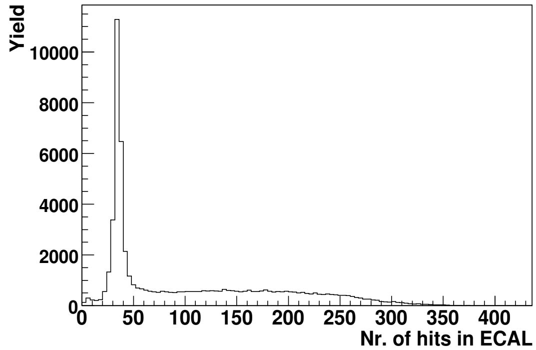

Figure 2: *Distribution of number of hits per event in the ECAL. The peak located at 30-40 units is originated by particles which do not shower in the ECAL calorimeter, and that are considered in this analysis.*

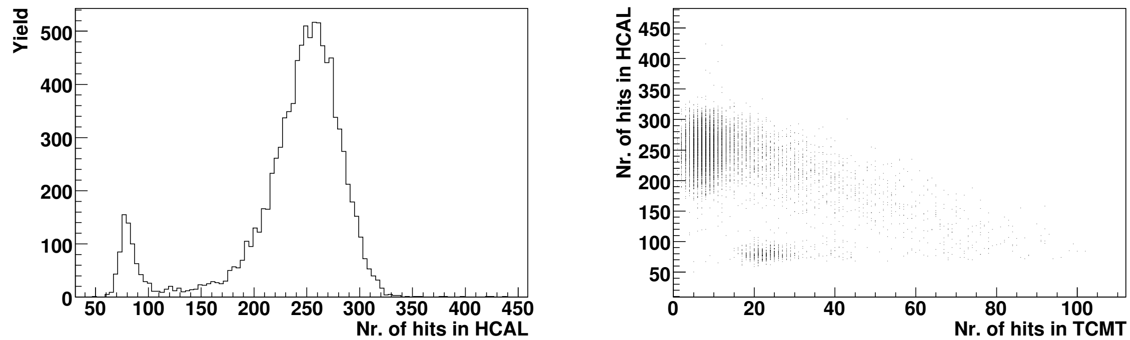

Figure 3: *Left panel: Distribution of number of hits per event in the AHCAL. Right panel: The number of hits per event in the AHCAL is shown versus the number of hits in the TCMT. Both distributions are presented after removing the events with showers starting in the ECAL, as described in the text.*

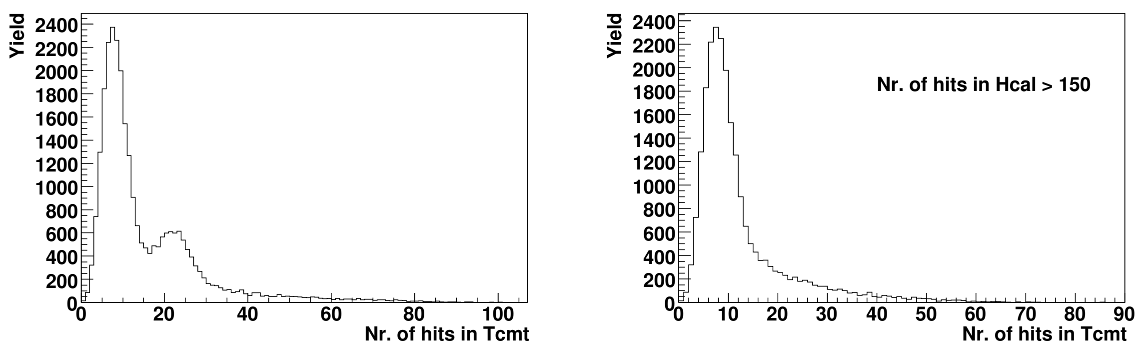

Figure 4: *The distribution of number of hits per event in the TCMT is presented without (left panel) and with (right panel) the selection of shower events in the AHCAL (number of hits per event in the AHCAL larger than 150). The bump at around 25 hits, and corresponding to MIP-like tracks, is removed.*

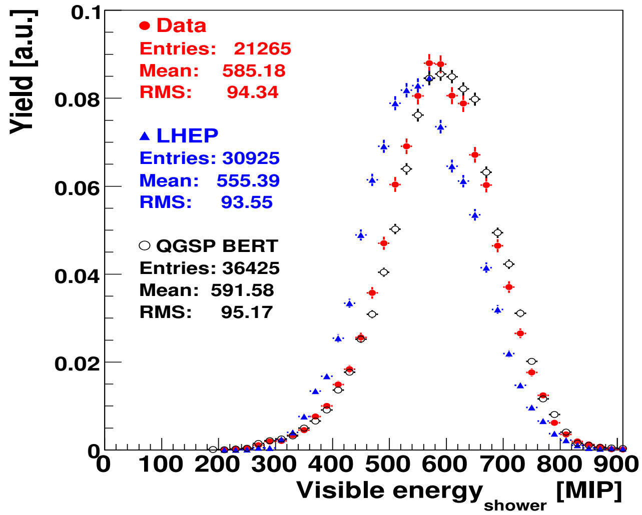

Figure 5: *Distribution of the shower energy (in MIP units) per event in the AHCAL for data and* GEANT4 *models considered in this analysis. All distributions are normalised to the corresponding total yield.*

remaining muon contamination in the analysed sample. Events with at least one and no more than 3 hits per layer in the TCMT, and with at least 15 (out of the total 16) layers which fullfill this condition, are assumed to be muon candidates and rejected. The contribution of this cut is negligible after requiring at least 150 firing cells per event in the AHCAL. The effect of lowering this cut (down to 120 hits per events) was found to be negligible.

The above mentioned cuts are used in the current analysis to define events with a hadron shower. Monte Carlo observables can have distributions different from the data, depending on the model used in the simulation. It was verified that the cuts optimised for the data can be applied to the Monte Carlo sample as well without biasing its distributions. Therefore, if not stated otherwise, the same cuts are applied in both data and Monte Carlo analysis. The errors of the presented distributions are statistical only, and are calculated assuming a Gaussian distribution for the measured quantity in the analysed bin.

4 Results

The total energy deposited by hadron showers in the AHCAL calorimeter varies among different GEANT4 models. The distribution of the reconstructed shower energy (in MIP units) for the considered models is shown in Fig. 5, and compared with the data. These differences are quantified in Table 1.

The observed difference in the reconstructed shower energy has to be taken into consideration while comparing the Monte Carlo simulations with the data.

	$\langle E_{sum} \rangle$ [MIP]	Deviation from data
Data	585	—
LHEP	555	5 %
QGSP_BERT	592	1 %

Table 1: *Average of the total energy deposited in the AHCAL, for data and the* GEANT4 *models investigated in this analysis, for an 18 GeV π^- run.*

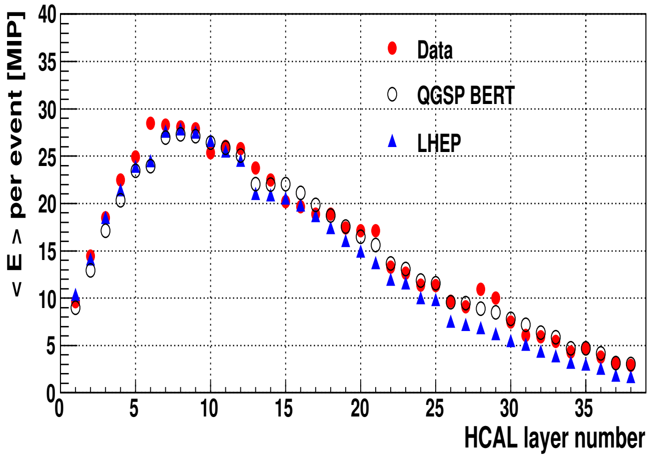

Figure 6: *Longitudinal energy profile of hadron showers in the AHCAL for the analysed 18 GeV π^- test-beam data.* GEANT4 *distributions are compared with the data.*

4.1 Lateral Energy Profiles of Showers

A shower developing in the calorimeter is reconstructed with respect to the incident track. For each shower event, the energy deposited in the i-th tile is localised (after aligning the AHCAL tiles to the impinging beam axis) in radial coordinate R according to

$$R_i = \sqrt{(x_i - x_{track})^2 + (y_i - y_{track})^2}\ . \tag{1}$$

In this formula, x_i (y_i) and x_{track} (y_{track}) are the x (y) coordinates of the tile and of the track impact point at the tile layer, respectively. The shower energy density, defined as the mean energy sum per event per unit of ring area, is then measured event by event in bins of the radial coordinate R.

The lateral profiles are presented in form of energy density distributions ρ_E as a function of the radial coordinate R. Rings of 10 mm width are built around the shower axis, and the energy density in the corresponding ring is measured. Note that in the following results the energy will be presented in MIP units.

The longitudinal energy development of showers typically shows an initial rise, reaches a maximum, which depends on the particle type, followed by a decay that is much less steep than the initial rise, as shown in Fig. 6. To investigate these three regions, where, in principle, interactions models can have different relative intensity, the core of lateral energy shower profiles is presented in Fig. 7 for three detector regions: layers 1 to 5 (i.e. rising slope of the longitudinal shower development), layers 6 to 10 (i.e. peak of the shower), and layers 11 to 38 (i.e. decreasing slope and tails of the shower). As expected, the lateral profiles exhibit a narrow core, representing the electromagnetic shower component, caused by π^0's produced in the shower development, and a halo with an exponentially decreasing intensity, caused mostly by non-electromagnetic shower component. Also shown are the GEANT4 Monte Carlo simulations using the models LHEP and QGSP_BERT. Of course, a meaningful comparison between data and Monte Carlo should not be performed with respect to the AHCAL layers, but instead considering the shower start location in the calorimeter as a reference. Nevertheless, profiles in different sections of the calorimeter are here presented as detector control plots. For data-Monte Carlo comparison, it is important to analyse also the tails of lateral profiles. This is shown in logarithmic scale in Fig. 8.

After integration over all the AHCAL layers, the lateral profile is presented in absolute MIP scale for both data and Monte Carlo in Fig. 9. The shower core is shown in linear scale in the left panel of the picture, while the shower tail can be better investigated in

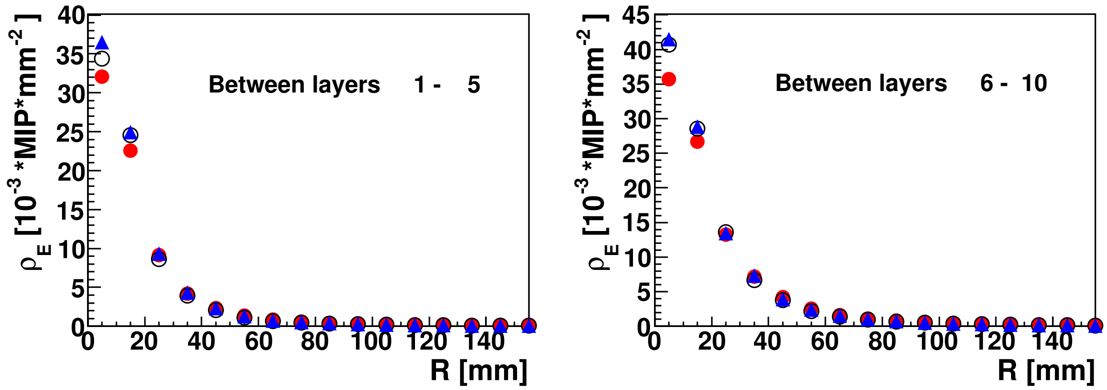

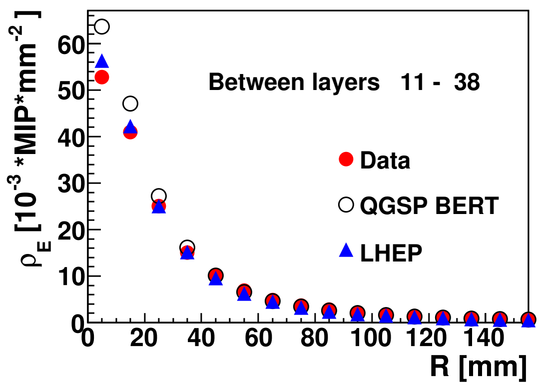

Figure 7: *The **core** of lateral energy profiles in MIP units is reconstructed in the three regions of the AHCAL selected as described in the text. Both the data and Monte Carlo simulations are shown.*

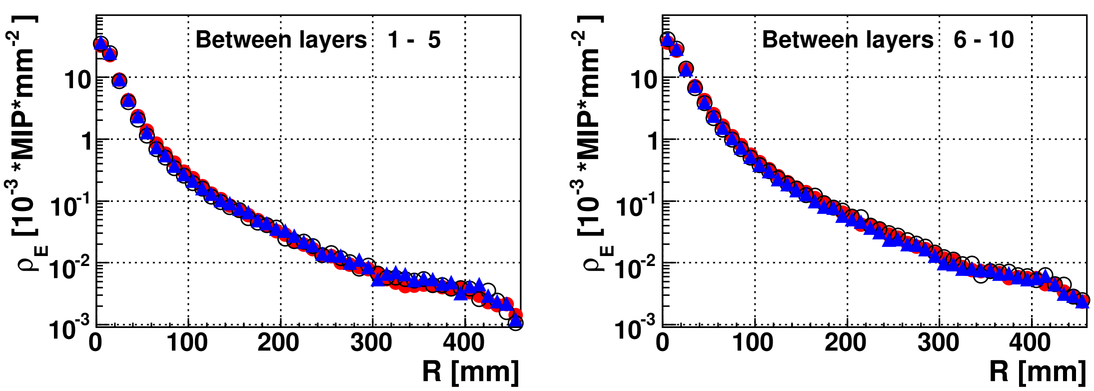

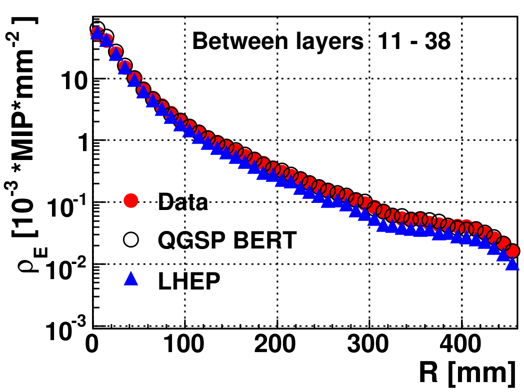

Figure 8: *The full extension of lateral energy profiles in MIP units reconstructed in the three regions of the AHCAL, selected as described in the text. Both the data and Monte Carlo simulations are shown. Profiles are presented in logarithmic scale to better investigate how well models reproduce the profiles tails.*

the right panel where the logarithmic scale was used. It appears that the profiles tail in the data is better reproduced by QGSP_BERT model.

As shown in Fig. 5, the total visible energy in the considered simulations differs from

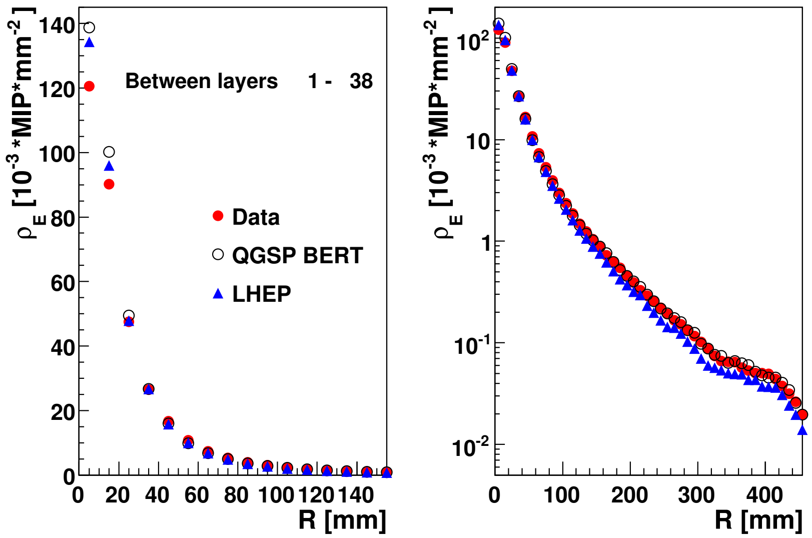

Figure 9: *Lateral energy shower profile in the whole AHCAL calorimeter. Left panel: The profile* ***core*** *is shown in linear scale. Right panel: The profile is shown in logarithmic scale to better investigate the tail energy content. Superimposed to the data are shown also* LHEP *and* QGSP_BERT *model simulations.*

the data. In order to possibly investigate where this difference is radially localised, the ratio of energy density for Monte Carlo over the data is calculated for each radial R bin, and presented in Fig. 10. A model energy bias, radially uniform (a global offset), should result in a flat prediction to data ratio for profiles versus R, which is not observed for both investigated models. In some bins of the tail, fluctuations larger than the calculated statistical uncertainty are visible. They should not affect the qualitative trend of the not flat ratio of Monte Carlo to data distributions. The observed structure, similar in both Monte Carlo models, is an indication of systematic effects, possibly induced by detector edges, which are under investigation.

4.2 Lateral Fractional Energy in Hadron Showers

The fractional energy deposition can be investigated as a function of the radial distance R from the incident test-beam primary track. It is calculated for every bin via energy integration from the lowest bin up to the R-bin, and then normalised to the total energy reconstructed in the detector. Exploiting the extended lateral granularity of the AHCAL prototype, the fractional energy deposition can be investigated in the whole lateral

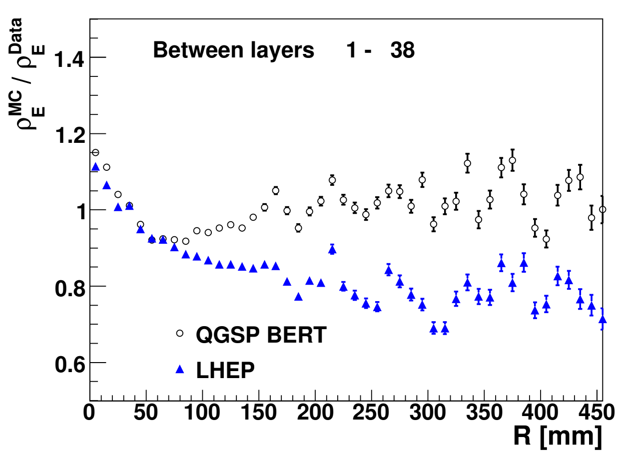

Figure 10: *The simulated energy density distributions (in the whole AHCAL calorimeter) are divided (bin by bin) by the data distribution. Global energy offsets in the simulations should result in flat distributions in terms of the radial distance* R*.*

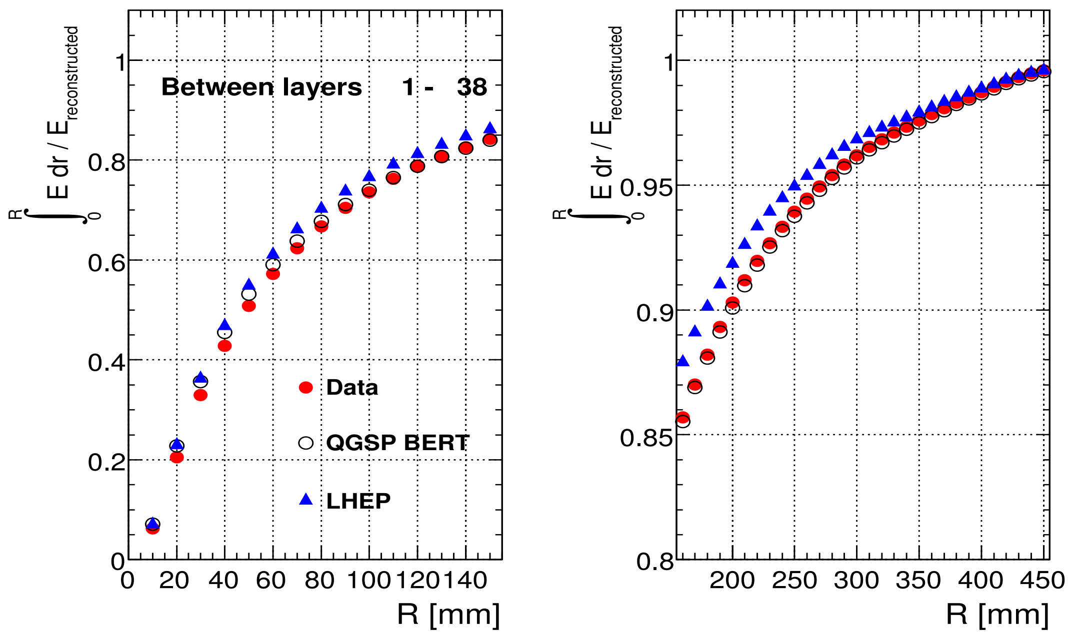

Figure 11: *The lateral fractional energy in the shower as a function of the radial distance from the primary test-beam track, for all AHCAL layers. Left panel:* ***Core*** *of the distribution, for data and for the two used* GEANT4 *models. Right panel:* ***Tail*** *of lateral fractional energy.*

shower development.

The comparison with the Monte Carlo models is shown in Fig. 11 for all AHCAL layers. QGSP_BERT model appears to better reproduce the fractional energy distribution in the shower tail, within the current data calibration and Monte Carlo tuning. The radius of showers which contains 95% of the total energy deposition was found to be around 27 cm for the data. The presented statistical uncertainties are correlated, since the fractional energy in a specific R-bin depends on the data sample used for the bin immediately lower.

4.3 Mean Hadron Shower Radius

For the International Linear Collider (ILC), several options for the hadronic calorimeter are considered. Previous studies (see for example [8]) indicate that the available Monte Carlo models show large variations of quantities which describe hadron showers in a scintillator and in a gas (RPC-based) hadronic calorimeter.

In this work the mean hadron shower radius is measured. The shower radius per event is defined in this analysis as the energy-weighted mean of hits radial coordinates

$$\langle R \rangle_{event} = \frac{\sum\limits_i E_i \cdot R_i}{\sum\limits_i E_i} \,, \tag{2}$$

where R is given in Eq. 1, and the sum is performed over all AHCAL cells i with energy $E_i > 0.5$ MIP which fired in the processed event. The distribution of the shower

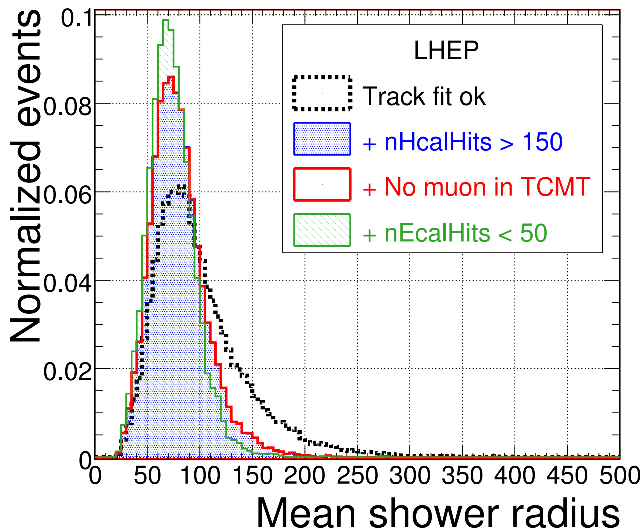

Figure 12: *The effect of the analysis cuts on the reconstructed hower radius distribution is shown for the* LHEP *model. The distribution is shown for events with hits in the AHCAL which have the energy $E > 0.5$ MIPs.*

radius values is then analysed, and compared with Monte Carlo predictions to possibly investigate the quality of hadron shower simulation by models.

The effect of the analysis cuts on the shower radius distribution is shown for the LHEP model in Fig. 12. The strongest effect is due to the cut on the number of AHCAL hits. This cut reduces the relative contribution of noise hits, which are uniformly scattered around the shower axis over all the calorimeter layers. Their inclusion in the analysis results in a larger reconstructed shower radius. The rejection of muon candidates in TCMT has a negligible effect, since the beam in Monte Carlo is a pure pion beam. The effect of the analysis cuts on the number of events, as well as on the mean and on the RMS of the shower radius distributions after applying the different cuts, are given in Tab. 2.

The mean shower radius distribution for data and the selected GEANT4 models is shown in Fig. 13. Note that LHEP produces few neutrons compared to cascade models, as in QGSP_BERT, hence the large difference compared to data. On the other side, QGSP_BERT produces too large showers due to a large number of neutrons with respect to data. This is reduced when properly correcting for the late coming neutrons which are not seen in data due to the signal saturation in scintillating tiles (Birks' law) and due to short signal shaping time in the readout electronics, as the Fig. 14 shows.

	LHEP			QGSP_BERT		
	ε_{cut}	$\langle R \rangle$	RMS	ε_{cut}	$\langle R \rangle$	RMS
Track fit OK	81 %	100	45	82 %	106	44
+nHcalHits > 150	42 %	80	27	55 %	92	32
+nEcalHits < 50	31 %	73	22	32 %	79	25

Table 2: *Efficiency of the analysis cuts, ε_{cut}, values of mean shower radius, and corresponding RMS for the used* GEANT4 *models.*

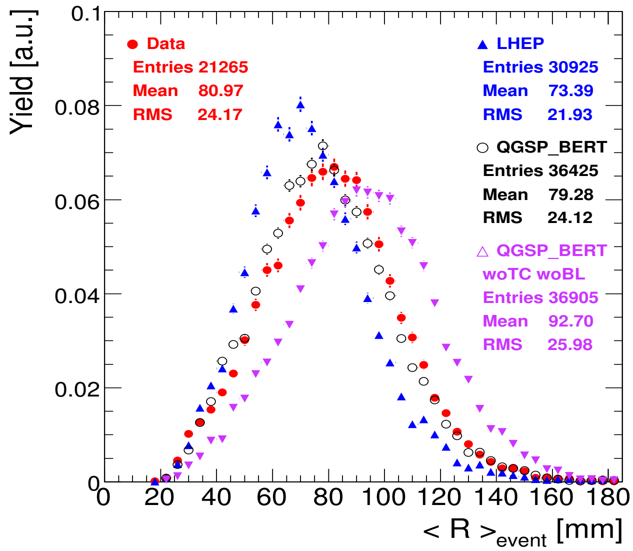

Figure 13: *Distribution of the shower radius per event reconstructed in the AHCAL for data and for the* GEANT4 *models considered in this analysis. All distributions are normalised to their corresponding total yield.*

5 Conclusions

Preliminary results on lateral development of hadron showers in the AHCAL were presented. Note that at the moment, only statistical uncertainties are considered, the systematics is still to be included.

The comparisons between 18 GeV π^- data and the two GEANT4 models, LHEP and QGSP_BERT, for the shower energy, transversal profiles, lateral fractional energy and mean shower radius were shown. The radius of the shower which contains 95% of the total energy deposition was found to be around 27 cm in data, whereas the showers have, on average, a mean radius of 8.1 cm.

Although none of the used GEANT4 models completely describe the data, it is clear that for a sensible data to Monte Carlo comparison one needs to use a proper treatment of the Monte Carlo, including specific physics and detector effects. It is also expected that the analysis of higher energies showers, where the dominance of one or other model is more clear, would shed more light in the understanding of the hadron shower physics.

The next analysis steps include the extraction of the shower components of the lateral

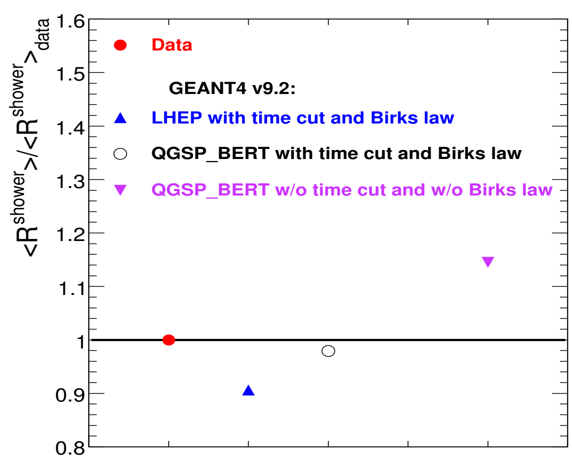

Figure 14: *The mean shower radius in the AHCAL obtained in* GEANT4 *Monte Carlo simulations shown normalised to the data.*

profiles, and the measurement of the profiles with respect to the start of the shower. In addition, the dependence of the profiles on the beam energy will be studied, once the higher energy runs are included. Possibly, also the effect of the type of the incident particle on the results will be investigated.

References

[1] CALICE Collaboration, *Preliminary Results From Hadron Shower Data with the CALICE Tile AHCAL Prototype*, CAN-011.

[2] J. Apostolakis et al., *Hadronic Shower Shape Studies in Geant4*, CERN-LCGAPP-2007-02 (2007).

[3] MOKKA web page, http://polywww.in2p3.fr/activites/physique/geant4/tesla/www/mokka/mokka.html.

[4] GEANT4 Collaboration, S. Agostinelli et al., GEANT4*: A Simulation Toolkit*, Nucl. Instrum. Meth. **A 506**, (2003) 250.

[5] J. B. Birks, *The Theory and Practise of Scintillation Counting*, Macmillan, New York (1964).

[6] B. Lutz, *AHCAL Longitudinal Profiles and Leakage*, talk given at the CALICE Collaboration Meeting, 18-20 Feb. 2009, Daegu, Korea.

[7] A. Lucaci-Timoce, *AHCAL: Status of Lateral Shower Shapes Analysis*, talk given at the CALICE Collaboration Meeting, 30 March 2009, Hamburg, Germany.

[8] G. Mavromanolakis and D. Ward, *Comparison of Hadronic Shower Packages*, LC-TOOL-2004-019, arXiv:physics/0409040.

6 Distributions Proposed for Release

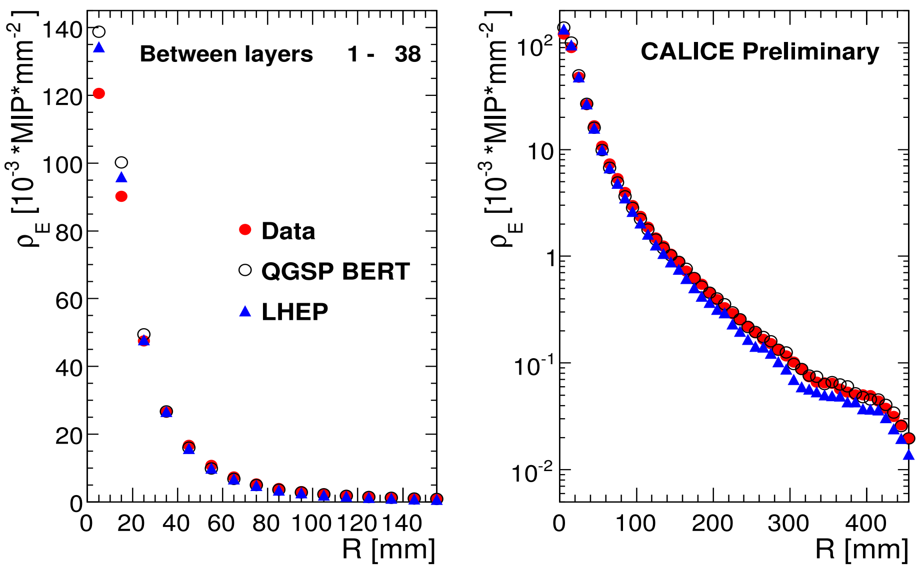

Figure 15: *Lateral energy shower profile in the whole AHCAL calorimeter. Left panel: The profile* ***core*** *is shown in linear scale. Right panel: The profile is shown in logarithmic scale to better investigate the tail energy content. Superimposed to the data are shown also the* LHEP *and* QGSP_BERT *model simulations.*

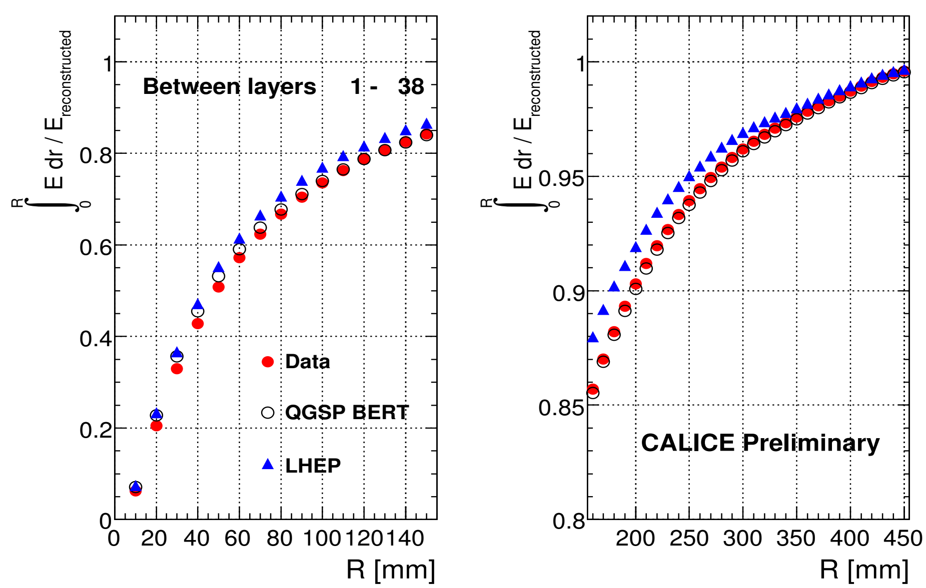

Figure 16: *The lateral fractional energy in the shower as a function of the radial distance from the primary test-beam track, for all AHCAL layers. Left panel:* ***Core*** *of the distribution, for data and for the two used* GEANT4 *models. Right panel:* ***Tail*** *of lateral fractional energy.*

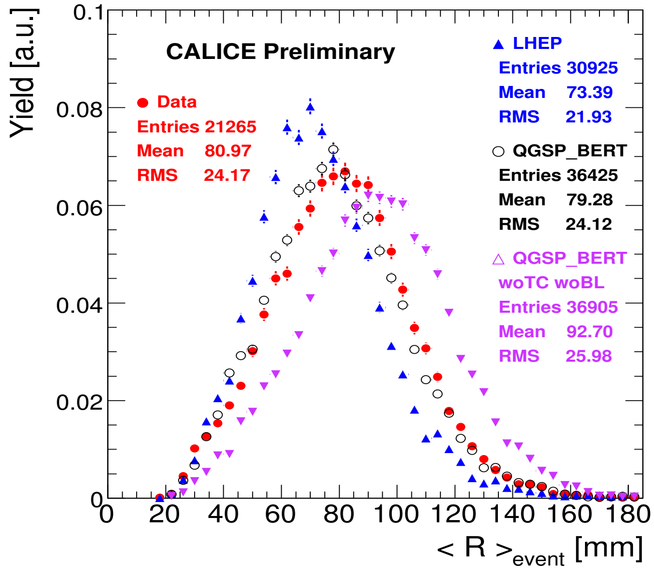

Figure 17: *Distribution of the shower radius per event reconstructed in the AHCAL for data and* GEANT4 *models considered in this analysis. All distributions are normalised to their corresponding total yield.*

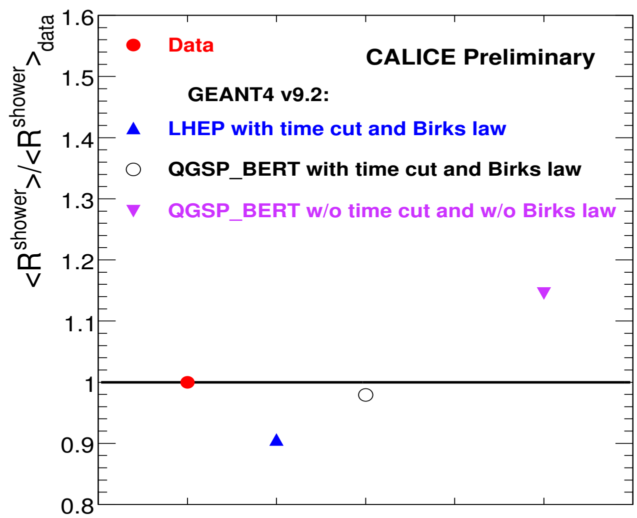

Figure 18: *The mean shower radius in the AHCAL obtained with the* GEANT4 *Monte Carlo simulations shown normalised to the data.*